pH-responsive relaxometric behaviour of coordination polymer nanoparticles made of a stable macrocyclic gadolinium chelate

Javier Aríñez-Soriano[a], Jorge Albalad[a], Arnau Carné-Sánchez[a], Célia S. Bonnet[b], Félix Busqué[c], Julia Lorenzo[d], Jordi Juanhuix[e], Maxwell W. Terban[f], Inhar Imaz[a], Éva Tóth*[b], Daniel Maspoch*[a,g]

Abstract: Lanthanide-containing nanoscale particles have been widely explored for various biomedical purposes, however, they are often prone to metal leaching. Here we have created a new coordination polymer (CP) by applying, for the first time, a stable Gd(III) chelate as building block in order to prevent any fortuitous release of free lanthanide(III) ion. The use of the Gd-DOTA-4AmP complex as a design element in the CP allows not only for enhanced relaxometric properties (maximum r_1=16.4 $mM^{-1}s^{-1}$ at 10 MHz), but also for a pH responsiveness (Δr_1 = 108% between pH 4 and 6.5), beyond the values obtained for the low molecular weight Gd-DOTA-4AmP itself. The CP is miniaturizable down to the nanoscale to form colloids that are stable in physiological saline solution and in cell culture media and does not show cytotoxicity.

Introduction

Magnetic resonance imaging (MRI) is a powerful diagnostic tool in medical science thanks to its non-invasive character and sub-millimetre spatial resolution. This success would not have been possible without the parallel development of contrast agents (CAs), which are substances capable of enhancing the intrinsic contrast of the technique and improve its anatomical resolution.[1] From the 80s, paramagnetic Gd(III) chelates have stood out for their excellent properties as CAs and their safe use in comparison to the toxic free Gd(III) ions.[2,3] Some of these Gd(III) chelates (*e.g.* Dotarem® and Prohance®) are currently commercially available and widely used in clinics. However, these substances are still affected by low sensitivity, lack of selectivity and low retention times, meaning that they are only effective in areas of high bioaccumulation. For this reason, there has been much interest in developing strategies to enhance the performance of this class of CAs.[4] Among the different strategies, a promising one is their nanostructuration, either by using them as building units to make new nanostructured materials or by attaching them onto pre-synthesized nanomaterials.[5] This approach provides the potential advantages of lowering the rotational tumbling of the Gd(III) chelates, enhancing the payload of Gd(III) ions per nanoparticle, and increasing the *in vivo* circulation time. To date, excellent results have been obtained by structuring Gd(III) chelates in dendrimers,[6] viral capsids,[7] proteins,[8] mesoporous silica,[9] polymeric self-assembled nanoparticles,[10,11] and liposomes.[12]

Nanoscale coordination polymers (CPs) and metal-organic frameworks (MOFs) are an alternative class of materials to be explored for nanostructuring these CAs. Prior to this work, some advances have been done in developing MRI CAs from CPs/MOFs.[13–15] These CAs have mainly been synthesized by the assembly of individual Gd(III) ions and polycarboxylic organic linkers.[16,17] However, since lanthanide-carboxylate-based CPs/MOFs typically lack stability in water and especially in body fluids, they would degrade when exposed to these media releasing the Gd(III) ions in their free toxic form. In addition, this lack of stability also prevents detailed relaxometry studies because of the interference of the leached free paramagnetic Gd(III) ions.

Herein, we present for the first time the incorporation of a Gd(III) macrocyclic chelate in the structure of a CP by connecting it through Zn(II) ions. Previous attempts made in our group to build up a CP using a Gd(III) macrocyclic chelate were focused on using the 1,4,7,10-tetraazacyclododecane-1,4,7,10-tetramethylenephosphonic acid (DOTP).[18] However, we found that the corresponding Gd-DOTP chelate did not react with most of metal ions (*e.g.* Zn(II), Ni(II), Co(II), Mn(II), Fe(III) and Mg(II)), presumably because the four phosphonate groups were coordinating the Gd(III) ions (Scheme 1).[19] In fact, the Gd-DOTP chelate reacted only with Cu(II) ions,[20] but through a mechanism that involved the replacement of the Gd(III) by the Cu(II) inside the DOTP macrocyclic cavity leaving the phosphonate groups free to coordinate to the replaced Gd(III) ions. In this work, we hypothesize that the introduction of a second functionality in the pendant arms of the macrocyclic ligand applied as linker should ensure the coordination of the Gd(III) inside the macrocyclic cavity while leaving the

[a] J. Aríñez-Soriano, J. Albalad, A. Carné-Sánchez, I. Imaz, Prof. D. Maspoch.
Catalan Institute of Nanoscience and Nanotechnology (ICN2).
CSIC and The Barcelona Institute of Science and Technology.
Campus UAB, Bellaterra, 08193 Barcelona, Spain.
E-mail: daniel.maspoch@icn2.cat

[b] C. S. Bonnet, Prof. E. Tóth.
Centre de Biophysique Moléculaire, CNRS, Université d'Orléans.
Rue Charles Sadron, 45071, Orléans, France.
E-mail: eva.jakabtoth@cnrs-orleans.fr

[c] Prof. F. Busqué.
Departament de Química, Universitat Autònoma de Barcelona.
Campus UAB, Bellaterra, 08193 Barcelona, Spain.

[d] Prof. J. Lorenzo.
Institut de Biotecnologia i Biomedicina (IBB).
Departament de Bioquímica i Biologia Molecular.
Campus UAB, 08193 Bellaterra, Spain.

[e] J. Juanhuix.
ALBA Synchrotron, Cerdanyola del Vallès, 08290 Barcelona, Spain.

[f] M. W. Terban.
Department of Applied Physics and Applied Mathematics.
Columbia University, New York, USA.

[g] Prof. D. Maspoch.
Institució Catalana de Recerca i Estudis Avançats (ICREA).
08010 Barcelona, Spain.

Supporting information for this article is given via a link at the end of the document.

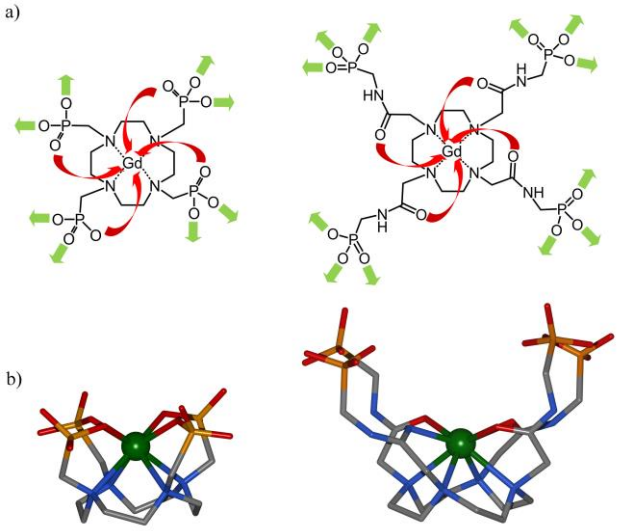

Scheme 1. (a) Gd-DOTP (left) and Gd-DOTA-4AmP (right) showing the coordination with Gd(III) (red arrows) and their potential coordination to a second metal ion (green arrows). (b) Three-dimensional conformation of Gd-DOTP (left) and Gd-DOTA-4AmP (right). Colour code: C (grey), N (blue), O (red), P (orange), Gd (green).

phosphonate groups free to coordinate to second metal ions and thus form the CP. For this reason, we have selected 1,4,7,10-tetraazacyclododecane-1,4,7,10-tetraacetamidomethylene phosphonic acid (DOTA-4AmP).[21] In contrast to DOTP, this macrocyclic ligand has two functionalities (amide and phosphonate groups) in each one of the four pendant arms. The four oxygen atoms of the amide groups along with the four ring nitrogen atoms chelate the Gd(III) ions inside the macrocyclic cavity, thereby allowing the Gd-DOTA-4AmP to have the four phosphonate groups free to coordinate with other metal ions forming CPs (Scheme 1). Importantly, the resultant CPs should also show more stability under aqueous conditions since phosphonates form stronger bonds with metals than carboxylates do.[22] Finally, another potential feature to be considered when using this macrocyclic linker is that, since the Gd-DOTA-4AmP chelate has been already proved to be endowed with pH dependent relaxivities,[21,23] its use could pave the way for the synthesis of nanostructured CPs that, in addition to enhanced CA properties, could behave as a pH-responsive contrast agent.

We demonstrate that bulk crystals of a three-dimensional CP with formula $Zn_{6.5}[Gd_3(H\text{-}DOTA\text{-}4AmP)_2(DOTA\text{-}4AmP)(H_2O)_3]\cdot 18H_2O$ (**1**) are formed when the pre-formed Gd-DOTA-4AmP chelate is diffused slowly with Zn(II) ions, whereas increasing the rate of this reaction produced amorphous 90 ± 30 nm-in-diameter CP nanoparticles. Here, Zn(II) ion was selected as the secondary metal ion for a series of key considerations: (i) its stability constant with macrocyclic ligands[24,25] is much lower than that of Gd(III)[26,27] and lower than those of other metals (*e.g.* Fe(III),[28] Cu(II),[24,25] etc.), preventing a competition with Gd(III) to occupy the macrocyclic cavity; (ii) its toxicity[29] is lower than other metals (*e.g.* Co(II),[30,31] Cu(II),[32,33] etc.), avoiding health risks in the case of disassembly of the structure inside the body; and (iii) it is a diamagnetic metal, so the performed relaxivity studies can be interpreted only in terms of the nanostructuration of its building block, the Gd-DOTA-4AmP chelate.[21] Importantly, the colloidal CP nanoparticles we have designed feature a high stability in physiological saline solution and in cell culture media, while they showed an increased r_1 relaxivity of 16 $mM^{-1}\cdot s^{-1}$ at 10 MHz (25°C, pH=7.4) when compared with that of the original Gd-DOTA-4AmP chelate. In addition, they amplify the relaxivity pH response (Δr_1 = 108%) that, at intermediate fields (20-40 MHz), doubles the one of the Gd-DOTA-4AmP chelate.

Results and Discussion

Synthesis and crystal structure of 1.

The macrocyclic ligand DOTA-4AmP was synthesized adapting a procedure reported in the literature.[21] This was then used as a linker to create the crystals of **1** following a two-step synthesis.[34] This synthesis consisted of first combining DOTA-4AmP with Gd(III) ions to obtain the corresponding metallomacrocyclic complex Gd-DOTA-4AmP showing non-coordinated phosphonic groups. Here, the Gd-DOTA-4AmP was prepared by adding dropwise a solution of gadolinium chloride hexahydrate in water into an aqueous solution of DOTA-4AmP adjusted to pH 10 (using 1M NaOH) under stirring at 70 °C. The pH of the mixture was kept at 10 using 1M NaOH throughout the addition. Then, the mixture was left at 70 °C under stirring for 18 h. Finally, the pH was adjusted to pH = 8 by the addition of concentrated HCl. The exact concentration of Gd(III) ions was determined by ICP-MS, and the final concentration of the GdDOTA-4AmP solution was adjusted to 20 mM by the addition of water. In a second step, an ethanolic solution of zinc acetate was layered onto the aqueous solution of Gd-(DOTA-4AmP). After two weeks, transparent octahedral crystals of **1** suitable for single crystal X-ray diffraction were collected.

Crystal structure of **1** was solved and refined in the tetragonal P42/n group (Table S1, in the Supporting Information). The asymmetric unit was found to contain three Gd-DOTA-4AmP units, in which the Gd(III) ion was confirmed to be chelated inside the macrocyclic cavity. This Gd(III) ions adopt a capped square antiprismatic geometry coordinated to the four ring nitrogen atoms, the four oxygen atoms of the amide functionalities and one water molecule at the capping position (Figure 1a). On the other hand, Zn(II) ions adopt a tetrahedral geometry coordinated to four O atoms of the phosphonate groups of the macrocyclic Gd-DOTA-4AmP units. In this structure, the three Gd-DOTA-4AmP of the asymmetric unit have differences in their geometry and coordination modes. According to the notation introduced by Harris *et al.*[35] (Figure S1a in the Supporting Information), the phosphonate groups of Gd1-DOTA-4AmP and Gd2-DOTA-4AmP show the binding mode [3.111] in one pendant arm and the binding mode [2.110] in the other three arms (Figure 1a and Figure S1b in the Supporting Information). The phosphonate groups of the Gd3-DOTA-4AmP unit adopt the binding mode [3.111] in one arm, [1.100] in another arm, and [2.110] in the two remaining arms (Figure S1b in the Supporting Information).

Overall, it is very interesting to note that the resulting structure can be analysed in terms of an inorganic framework

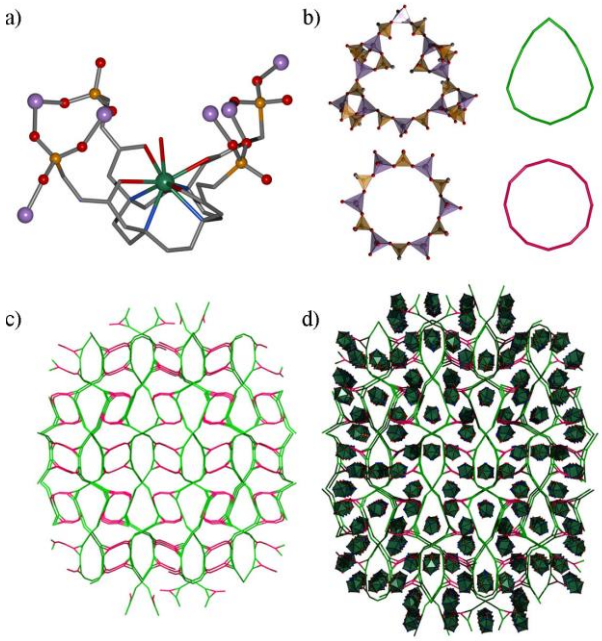

Figure 1. (a) Gd-DOTA-4AmP unit found in **1**. (b) Egg-shaped 32-membered ring and circular 24-membered ring found in **1**. (c) View of the three-dimensional Zn(II)-PO_3 network resulting from the assembly of the two types of rings along *a* axis. (d) Identical view of **1** including the Gd-DOTA-4AmP units. Colour code: C (grey), N (blue), O (red), P (orange), Gd (green), Zn (purple).

since the ···Zn(II)-PO_3-Zn(II)-PO_3··· linkages extend along the three dimensions. In this framework, the basic units are tri-winged paddle wheel Zn(II) units, which are formed by two Zn(II) ions bridged by three phosphonate groups (Figure S2 in the Supporting Information). The assembly of these Zn(II) units generate two types of $Zn_xP_xO_{2x}$ rings (Figure 1b), one circular 24-membered ring ($Zn_6P_6O_{12}$, 10.9 × 10.3 Å) and one egg-shaped 32-membered ring ($Zn_8P_8O_{16}$, 16.3 × 5.6 Å). The size of these rings is relatively larger than other $Zn_xP_xO_{2x}$ rings previously reported.[36] Figure 1c shows the three-dimensional Zn(II)-PO_3 network resulting from the assembly of these two types of rings. Importantly, the Gd-DOTA-4AmP units are enclosed in the "hypothetical" channel system of this framework, resulting in a more compact structure (Figure 1d) in which guest water molecules are hydrogen-bonded with the oxygen atoms of the different phosphonate groups.

Synthesis and characterization of the Zn-Gd-DOTA-4AmP nanoparticles.

Any attempt to miniaturize **1** and form colloidal crystalline nanoparticles by means of different techniques (*e.g.* hydrothermal synthesis, fast mixing of reactants, emulsions, etc.) failed. Here, all trials let to the formation of amorphous Zn-Gd-DOTA-4AmP nanoparticles. In fact, by reproducing exactly the same synthesis, but instead of a slow diffusion of both solutions, we rapidly mixed them, amorphous Zn-Gd-DOTA-4AmP nanoparticles were immediately formed. These nanoparticles were then purified by centrifugation and washed several times with ethanol and water, and finally redispersed in water. The resulting white colloid showed a good stability (Figure 2a), and the first reversible flocculation traces only appeared after one day. Field-Emission Scanning (FESEM) and Transmission (TEM) electron microscopy images of the colloid demonstrated the formation of rounded nanoparticles (Figure 2b-d and Figure S4 in the Supporting Information) with a size of 90 ± 30 nm (calculated from TEM images by averaging the diameter of at least 150 particles from images of different areas of the same sample).

To gain more information about the structural-chemical correspondence between Zn-Gd-DOTA-4AmP nanoparticles and the crystalline structure of **1**, we compared the results obtained using different characterization techniques. First, ICP-MS analysis performed on the nanoparticles showed a Zn:Gd proportion of 2.07, which is consistent with that of the crystalline structure (Zn:Gd = 2.16). This result confirms that the proportion between both metal ions is analogous in both materials. Second, elemental analysis performed on the nanoparticles agreed with the formula $Zn_{6.5}[Gd_3(H\text{-}DOTA\text{-}4AmP)_2(DOTA\text{-}4AmP)(H_2O)_3]\cdot 18H_2O$ (Table S2 in the Supporting Information). Third, both infrared (FT-IR) spectra (Figure S5 in the Supporting Information) and thermogravimetric analysis (TGA) (Figure S6, in the Supporting Information) done on the nanoparticles and **1** matched. Here, the IR spectra confirm the coordination of the phosphonate groups of Gd-DOTA-4AmP to the Zn(II) metal ions, as evidenced by the presence of two strong peaks at 1070 cm^{-1} and 992 cm^{-1}.[37] TGA showed a first weight loss of 9.1 % for **1** and 10.6 % for Zn-Gd-DOTA-4AmP nanoparticles in the range 35-275 °C, which was attributed to the loss of all guest water

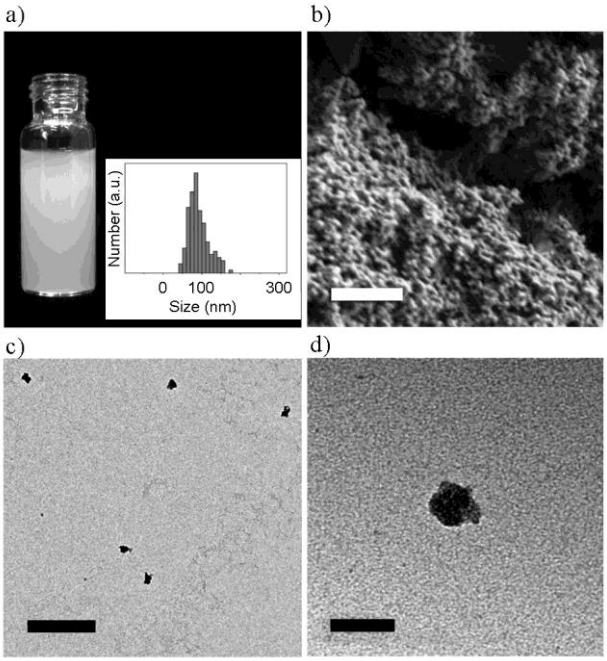

Figure 2. (a) Photograph of the colloidal suspension of Zn-Gd-DOTA-4AmP nanoparticles and the size distribution (inset). (b) SEM and (c and d) TEM images of Zn-Gd-DOTA-4AmP nanoparticles. Scale bars: (b) 1 µm, (c) 500 nm and (d) 100 nm.

molecules (theoretical = 10.5 % considering molecular formula of **1**). Decomposition of **1** and Zn-Gd-DOTA-4AmP nanoparticles occurs in the range of 275-740 °C in a single step (Figure S6 in the Supporting Information). Finally, ^{31}P MAS NMR solid-state measurements using Eu(III) instead of Gd(III) (**1** and **1**-Eu are isostructural; see Figure S3 and Figure S5 in the Supporting Information)[38,39] confirmed that the peak shift to higher fields and its widening due to the inclusion of Eu(III) in the DOTA-4AmP ligand was maintained in the case of Zn-Eu-DOTA-4AmP nanoparticles and in crystals of **1**-Eu. This result confirmed the presence of the lanthanide(III)-DOTA-4AmP unit in both materials (Figure S7 in the Supporting Information).

We also collected X-Ray total scattering pair distribution function (PDF) data for both samples. PDF analysis is an excellent technique to access structural information about materials in which disorder or crystallite size broadening effects limit the use of conventional Bragg crystallographic techniques.[40] Because of this, PDF analysis has recently been applied in CP/MOFs to study conformational changes[41] or to identify the correct structural features in MOF nanocrystals.[42] Figure 3 shows the results of these measurements as the PDF, G(r) function of each sample. G(r) provides the real-space probability of finding a pair of atoms at a distance r relative to the average atomic density in an isotropic sample; that is, it is a weighted histogram of atom-atom distances in a structure. The presence of peaks in the case of **1** at r > 5 Å (Figure 3a and Figure S8 in the Supporting Information) indicates long-range order and agrees with the Bragg diffraction observed in the PXRD measurements (Figure S3 in the Supporting Information). On the other hand, Zn-Gd-DOTA-4AmP nanoparticles appear diffuse for r > 5 Å, demonstrating the loss of long-range order as a consequence of the miniaturization process. However, a careful analysis (using PDFgui software, Figure S9 in the Supporting Information)[43] of the peaks at low distances (r) revealed that **1** and Zn-Gd-DOTA-4AmP nanoparticles present a very similar pattern (Figure 3a). Figure 3 correlates the peak positions of G(r) for both materials with the average atomic distances extracted from the crystalline structure of **1**. Their similarity confirms that the main building blocks forming the crystal structure of **1** are also present in the nanoparticles. The loss of the peak at 5.43 Å shows that disordering may develop between the Gd(III) ion and the Zn(II) ion distance upon miniaturization. Additionally, the presence of two broader features beyond 5 Å (Figure S8 in the Supporting Information) show that a small degree of structural coherence remains up to about 10 Å.

To this end, altogether these techniques confirmed that, even though the Zn-Gd-DOTA-4AmP nanoparticles do not show a long range structural ordering, their composition and chemical connectivity at a short range is comparable to those found in the structure of **1**.

Relaxometric measurements.

Reliable relaxometry studies of any material need to be done in a stable nanoparticle colloid. Thus, we first studied the stability of these nanoparticles in physiological saline solution (NaCl, 0.9%). For this, as-synthesised Zn-DOTA-4AmP nanoparticles were first centrifuged and redispersed in water three times and finally redispersed in the medium of study to form a stable colloid. Exposure of this sample to saline solution at pH = 5.5, 7.4, and 8.5 and at T = 37.5 °C led to negligible leaching of total Gd(III): 1.7 %, 1.2 % and 1.8 % in the first 10 minutes, and 3.6 %, 1.3 % and 1.8 % after 10 hours, as determined by ICP-MS (Figure S10 in the Supporting Information).

a)

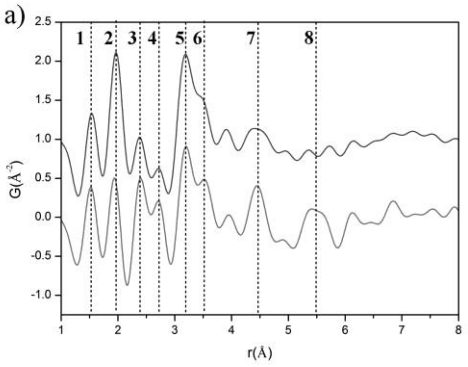

b)

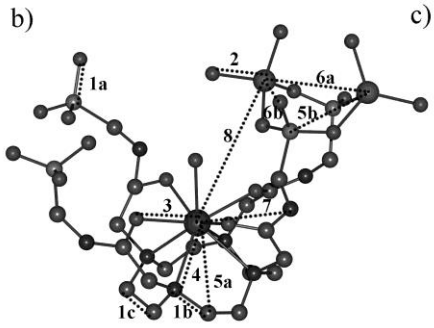

c)

Peak	Peak position (Å)	Contribution to the peak	Distance in 1 (Å)
1	1.50	**1a.** P-O	1.52
		1b. N-C	1.50
		1c. C-C	1.50
2	1.91	Zn-O	1.90
3	2.40	Gd-O	2.37
4	2.60	Gd-N	2.61
5	3.26	**5a.** Gd-C	3.42
		5b. Zn-P	3.17
6	3.60	**6a.** Zn-Zn	3.69
		6b. Zn-O	3.64
7	4.48	Gd-N	4.45
8	5.43	Gd-Zn	5.47

Figure 3. a) Pair distribution function G(r) of **1** (bottom) and Zn-Gd-DOTA-4AmP nanoparticles (top). b) Characteristic distances indicated in the PDF. c) Pair atom correlations contributing to the peaks in the PDF with their corresponding average crystallographic distance in **1**.

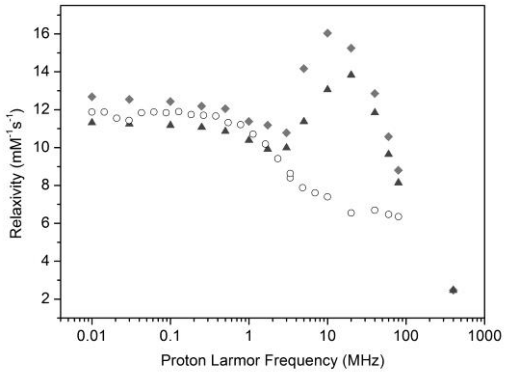

Figure 4. NMRD profiles of a colloidal suspension of Zn-Gd-DOTA-4AmP nanoparticles in saline solution (NaCl 0.9 %) at pH 7.4 at 25°C (light grey diamond) and at 50 °C (dark grey triangle) and Gd-DOTA-4AmP complex in saline solution (NaCl 0.9 %) at pH 7.4 at 25°C (empty circle).

The form in which the small amount of Gd(III) is released during this degradation was studied by mass spectrometry (ESI-TOF) and ^{1}H-NMR spectroscopy. To study the former, we analysed the supernatants resulting from the degradation experiments using ESI-TOF. From this analysis, we found species corresponding to [^{158}Gd-4H-DOTA-4AmP]$^-$= 930.1, [^{160}Gd-4H-DOTA-4AmP]$^-$= 932.1, [^{157}Gd-4H-DOTA-4AmP]$^-$= 929.1, [^{156}Gd-4H-DOTA-4AmP]$^-$= 928.1 and [^{155}Gd-4H-DOTA-4AmP]$^-$= 927.1 (Figure S11 in the Supporting Information), confirming that Gd(III) ions are still chelated when they are leached. In addition, studying the supernatant resulting from incubating a colloid of Zn-Eu-DOTA-4AmP nanoparticles (strongly relaxing Gd(III) ions were replaced by Eu(III) ions that allow for NMR observations; *vide supra*) to acidic D_2O conditions by ^{1}H-NMR further corroborated that lanthanide ions are still chelated during the degradation of the nanoparticles. Indeed, the ^{1}H-NMR spectrum showed the presence of the characteristic eight resonances of equal intensity corresponding to the chelate Eu-DOTA-4AmP (Figure S12 in the Supporting Information), but not those signals corresponding to free DOTA-4AmP. These results are in agreement with cytotoxicity assays conducted with two cell lines, Hep G2 and MCF-7. Both cells showed good viability (75 % for Hep G2 and for MCF-7) when incubated for 24 h with Zn-Gd-DOTA-4AmP nanoparticles, even at [Gd] = 200 µM. This lack of cytotoxicity for the nanoparticles is attributed to the eventual release of the Gd-DOTA-4AmP species non-toxic to cells instead of the free Gd(III) ion. Indeed, identical toxicity experiments performed on the Gd-DOTA-4AmP chelate showed that Gd-DOTA-4AmP exhibits similar viabilities (69 % for Hep G2 and 67 % for MCF-7). Clearly, the lack of cytotoxicity does not warrant *in vivo* non-toxicity. Also, the presence of phosphonate groups often drives to bone accumulation of such agents.[44] Nevertheless, they still might be helpful in small animal studies without causing acute toxicity, as it has been evidenced by the successful use of Gd-DOTA-4AmP for pH-mapping of mouse kidney[45] or rat glioma.[46]

Relaxometry properties were investigated by ^{1}H nuclear magnetic relaxation dispersion (NMRD) profiles in the frequency range 10 kHz ≤ v ≤ 400 MHz using a colloidal suspension of the Zn-Gd-DOTA-4AmP nanoparticles in saline solution. The suspension was stable throughout the measurement without addition of surfactants or thickeners that can interfere. The relaxivity r_1 profiles as a function of the magnetic field at pH = 7.4 at 25 °C and 50 °C show an increase at intermediate magnetic fields, reaching a maximum of r_1 at 10 MHz and 25 °C (r_1 = 16 mM^{-1}s^{-1}) (Figure 4). This is characteristic of slowly rotating species and enables to reach more than two times higher relaxivities than that of the discrete Gd-DOTA-4AmP complex at the same field and temperature (r_1 = 7.4 mM^{-1}s^{-1}).

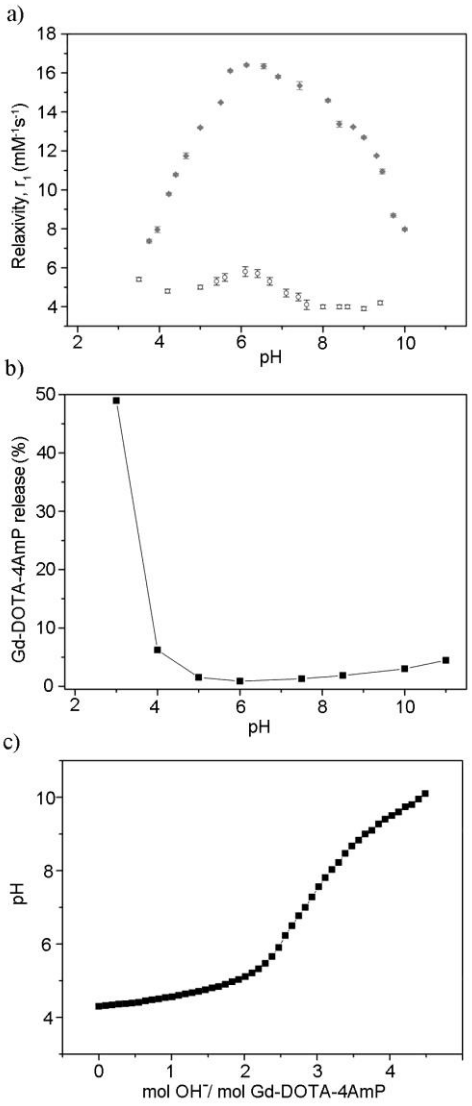

Figure 5. (a) pH dependence of the relaxivity of a colloidal suspension of Zn-Gd-DOTA-4AmP nanoparticles (filled diamond) and Gd-DOTA-4AmP complex (empty circle) measured at 20 MHz (25 °C). (b) Gd-DOTA-4AmP release (wt. %) for Zn-Gd-DOTA-4AmP nanoparticles at the pH range of study. (c) Potentiometric titration of a colloidal suspension of Zn-Gd-DOTA-4AmP nanoparticles.

Figure 4 also shows that the relaxivity slightly decreases with temperature, conversely to what was observed for the previously reported CAMOF-1,[18] where mean proton exchange was the limiting factor. The temperature-dependence of the relaxivities of Zn-Gd-DOTA-4AmP nanoparticles indicates that the relaxivity is not limited by proton exchange.

pH-dependent relaxometric study.

The pH dependence of r_1 of Zn-Gd-DOTA-4AmP nanoparticles was studied at 20 MHz in the pH range between 4 and 10 (Figure 5a). This pH range was selected to avoid leaching of either Gd-DOTA-4AmP or Zn(II) ions. Indeed, the release is less than 3.0 % in weight at 4 < pH < 10, however a burst release of the complex was observed at pH ≤ 4, indicating a fast degradation of the nanoparticles below pH 4 (Figure 5b). In consequence, relaxometric data were collected in the pH range 4-10 by starting with a colloidal suspension of these nanoparticles in saline solution at pH = 7.4 and with a Gd(III) concentration of 5.4 mM. The pH was stepwise lowered to 4 and then increased to 10 by the addition of small quantities of hydrochloric acid and sodium hydroxide, respectively, after which the pH and T_1 were immediately measured. The concentration of Gd(III) was corrected after each addition of concentrated acid/base to calculate r_1. Identical r_1 values were obtained when starting the measurements from a colloidal suspension with a pH initially set at 4 and raising it with sodium hydroxide, confirming the reversibility of the pH dependence of Zn-Gd-DOTA-4AmP nanoparticles. The plotted data have the shape of an asymmetric inverted parabola (Figure 5a). The r_1 values steeply increase from pH = 4 (r_1 = 7.9 $mM^{-1}s^{-1}$) to pH = 6 (maximum r_1 = 16.4 $mM^{-1}s^{-1}$), then steadily decrease reaching a value of r_1=8 $mM^{-1}s^{-1}$ at pH = 10. For direct comparison, we also repeated the pH dependence study for the Gd-DOTA-4AmP complex.[21] r_1 values increase from pH = 4 (r_1 = 4.8 $mM^{-1}s^{-1}$) up to pH = 6 (maximum r_1 = 5.8 $mM^{-1}s^{-1}$), followed by a decrease to reach a minimum at pH = 9 (r_1 = 3.9 $mM^{-1}s^{-1}$). As Figure 5a evidences, the use of the nanoparticle amplifies the pH-dependent relaxivity changes at this frequency. Indeed, for Zn-Gd-DOTA-4AmP nanoparticles, the difference between the maximum (r_1 = 16.4 $mM^{-1}s^{-1}$; pH 6) and the minimum (7.9 $mM^{-1}s^{-1}$; pH 4) relaxivity values corresponds to a factor of two (Δr_1 = 108 %), while for Gd-DOTA-4AmP, the difference between the maximum (r_1 = 5.8 $mM^{-1}s^{-1}$) and the minimum (r_1 = 3.9 $mM^{-1}s^{-1}$) is a factor of 1.5. This is nevertheless a slightly smaller amplification than what has been observed for Gd-DOTA-4AmP conjugated to a G5-PAMAM dendrimer (Δr_1 = -122 % between pH 6 and 9).[47] Evidently, the amplification of the pH response by nanoscale systems such as our CP or the G5-PAMAM dendrimer operates only at intermediate fields, where the effect of slow rotation on proton relaxivity is observable.

Sherry and co-workers showed with potentiometric and relaxometric studies that the phosphonates of the pendant arms were responsible of the unique pH-responsive behaviour of Gd-DOTA-4AmP.[21] They concluded that the protons of the Gd(III)-bound water molecule undergo a prototropic exchange with the bulk solvent which is catalysed by the phosphonate groups located close enough to the coordinated water. In particular, they could derive that the diprotonated complex has the maximal effect on the measured relaxivity and was responsible for the relaxivity peak at pH 6.3. They have also shown that converting these phosphonate groups to phosphonate esters eliminates the pH responsive behaviour.[48]

It is remarkable that the pH dependence profile of the relaxivity is preserved when Gd-DOTA-4AmP is part of a coordination polymer framework, despite the fact that most of the phosphonate oxygens are involved in coordination bonds to the Zn(II) cations. We have proved that the coordination polymer is not destroyed in the pH range 4-10 (see above). We can thus hypothesize that three possible mechanisms could account for the pH responsiveness of the nanoparticles, which can take place simultaneously. First, the pH dependence in the nanoparticles can be attributed to non-coordinating phosphonate groups on the surface of the nanoparticles. Second, intrinsic defects of any framework could also assure the presence of a number of non-coordinating phosphonate groups also in the interior of the nanoparticles. Finally, it has been described that coordinated oxygen atoms of the phosphonate groups can also accept protons,[49] making possible their protonation and the catalysis of the prototropic water exchange on the Gd(III) centres as formulated by Sherry.

By potentiometry, Sherry *et al.* determined four protonation constants for the monomer Gd-DOTA-4AmP complex, which are $\log K_{H1\text{-}4}$ = 7.20, 6.47, 6.03 and 5.36, respectively. In order to gain some information about the protonation scheme of the Zn-Gd-DOTA-4AmP nanoparticles, we have titrated a solution of the nanoparticles (5.4 mM in Gd(III)) by adding increasing amounts of 1 M NaOH. The titration curve shows that protonation occurs in a larger range (pH 4 to 10, Figure 5c) than what was observed for the monomer, which is not surprising as many protonation sites are in close proximity, and the Zn-Gd-DOTA-4AmP nanoparticle is expected to behave as a polyelectrolyte. This implies that the protonation of one site strongly influences the protonation of neighbouring sites. As a result, the protonation steps extend on a larger pH-range, instead of being characterized by discrete protonation constants. This site-binding model explains the characteristic broadening of the titration curve of polyelectrolytes with respect to the one of a corresponding monoprotic acid or base.[50]

Although it is impossible to extract protonation constants from the titration curve, it unambiguously indicates that in average, there are several protonation sites per Gd-DOTA-4AmP unit in the nanoparticles. It implies that protonation occurs also within the interior of the framework. This is an interesting finding since it shows that these nanoparticles can accept a large quantity of protons without the destruction of the coordination polymeric network. We note that metal coordination of protonated phosphonate oxygens has been previously reported.[49] Based on these results, we can conclude that the possibility to protonate the phosphonate oxygens even within the nanoparticles explains why the pH-dependent relaxivities are retained.

Conclusions

We have created a bimetallic Zn(II)- and Gd(III)-based coordination polymer (CP) by using, for the first time, a macrocyclic chelate (Gd-DOTA-4AmP) as building block. This design element warrants stable complexation of the lanthanide ion, even in case of partial disassembly of the polymeric network. This coordination polymer is miniaturizable to the nanometer scale (90 ± 30 nm) to form stable colloids, preserving its structural coherence up to about 10 Å. The colloid is stable in saline solution at physiological pH, in cell culture media; and it does not show cytotoxicity. The Zn-Gd-DOTA-4AmP nanoparticle has a maximum r_1 relaxivity of 16.4 $mM^{-1}s^{-1}$ at pH 6 and 10 MHz. It retains the pH dependence profile of the monomer in the pH range 4-10, with a double relaxivity response to pH change (Δr_1 = 108%) as compared to the monomer Gd-DOTA-4AmP (Δr_1 = 50%). Furthermore, we have demonstrated by potentiometric measurements that the Zn-Gd-DOTA-4AmP CP nanoparticles behave as a polyelectrolyte, accepting several protons per Gd-DOTA-4AmP unit without destroying the CP framework.

This proof of concept study shows that Gd(III)-chelates can serve as building blocks to create stable MOFs/CP. Such systems can be explored to enhance the relaxivity or pH dependence properties in view of their potential use in MRI diagnostics.

Experimental Section

General considerations.

All chemical reagents and solvents were purchased from commercial sources and used as received without further purification. NMR spectra were recorded on a Bruker Avance DPX-250 spectrometer and Bruker AMX-400 Wide Bore for liquid and solid-state samples respectively. Mass spectra were acquired on a micrOTOF-QII ESI-MS instrument. Purity of all bulk material batches was confirmed by X-ray powder diffraction (XRPD) patterns collected on an X'Pert PRO MPD analytical diffractometer (Panalytical) at 45 kV, 40 mA using Cu Kα radiation (λ 1.5419 Å), and compared with single crystal simulated patterns. Thermogravimetric analyses were performed under nitrogen flow using a STA 449 F1 Jupiter–Simultaneous TGA-DSC from NETZSCH with a heat rate of 5°C/min. IR spectra were recorded in transmission mode on a Bruker Tensor 27FTIR equipped with a Golden Gate diamond ATR cell. Elemental Analysis measurements were performed on a Flash EA 2000 CHNS, Thermo Fisher Scientific analyser. Inorganic Elemental Analysis measurements were performed on an ICP-MS 7500ce, Agilent Technologies. Scanning electron microscope images were acquired on a FEI Quanta 650F working at an accelerating voltage of 2 kV and a beam current of 50 pA. Transmission electron microscope images were acquired on a JEOL JEM-1400 working at an accelerating voltage of 120 kV.

Synthesis of Gd-DOTA-4AmP and Eu-DOTA-4AmP.

First, a solution of DOTA-4AmP (354 mg, 396 µmol) in water (8 mL) was prepared and the pH was adjusted at 10 by cautious addition of 1M NaOH. Then, a solution of gadolinium chloride hexahydrate was prepared (147 mg, 396 µmol) in water (2 mL). Gadolinium chloride solution was added drop by drop into the stirring DOTA-4AmP solution warmed at 70 ºC. The pH of the stirring mixture was kept at 10 by addition of concentrated NaOH (1M) during the addition process. Notice that, after each addition of gadolinium chloride into the DOTA-4AmP solution, a white precipitate appears at first, but it is dissolved after some minutes, indicating that Gd-DOTA-4AmP is being formed. The absence of free Gd(III) in the stirring mixture was also monitored by xylenol orange test.[51] The addition of gadolinium chloride was stopped after the xylenol test showed the persistent presence of free gadolinium. Then, the mixture was left at 70 °C under stirring for 18 h. Finally, the pH was adjusted to pH = 8 by the addition of concentrate HCl. The exact concentration of Gd(III) ions was determined by ICP-MS, and the final concentration of the Gd-DOTA-4AmP solution was adjusted to 20 mM by the addition of water. The same procedure was followed for the synthesis of Eu-DOTA-4AmP but using europium chloride hexahydrate instead of gadolinium chloride.

Synthesis of 1 and 1-Eu.

A solution of zinc acetate dihydrate in ethanol (4 mL, 11.3 mM) was carefully layered onto a Gd-DOTA-4AmP aqueous solution (4 mL, 5.2 mM) in a 9 mL glass vial. This glass vial containing the liquid diffusion was capped and left undisturbed at room temperature for two weeks. After that, transparent octahedral crystals of **1** appeared on the walls and at the bottom of the vial. To recover crystals of **1**, the liquid phase was exchanged by fresh EtOH/water mixture (50:50) and the vials sonicated in an ultrasounds bath at 0 °C to detach the crystals from the glass walls. The process was repeated two more times, and the crystals were finally kept under pure water. The same procedure was followed for the synthesis of **1**-Eu but using an aqueous solution of Eu-DOTA-4AmP instead of Gd-DOTA-4AmP.

Synthesis of Zn-Gd-DOTA-4AmP and Zn-Eu-DOTA-4AmP nanoparticles.

A solution of zinc acetate dihydrate in ethanol (4 mL, 11.3 mM) was rapidly added onto a Gd-DOTA-4AmP aqueous solution (4 mL, 5.2 mM) under stirring (900 rpm) at room temperature. Inmediately after this addition, the appearance of a white solid was observed, and the mixture was left under stirring for 12 h. To recover Zn-Gd-DOTA-4AmP nanoparticles, the solid was precipitated by centrifugation (44,000 RCF, 10 min) and washed four times with EtOH/water mixture (50:50) and finally redispersed in pure water. The same procedure was followed for the synthesis of Zn-Eu-DOTA-4AmP nanoparticles but using an aqueous solution of Eu-DOTA-4AmP instead of Gd-DOTA-4AmP.

X-Ray Crystallography.

Crystallographic data for **1** were collected at 100 K at XALOC beamline[52] at ALBA synchrotron (λ = 0.88557 Å). These data were indexed, integrated and scaled using XDS program.[53] Absorption correction was not applied. The structure was solved by direct methods[54] and subsequently refined by correction of F2 against all reflections using SHELXS2013 and SHELXL2013 within the WinGX package.[55] All non-hydrogen atoms were refined with anisotropic thermal parameters by full-matrix least-squares calculations on F2 using SHELXL2013. Hydrogen atoms were inserted at calculated positions and constrained with isotropic thermal parameters. The hydrogen of the crystal lattice water molecules present in the structure were not located on Fourier map, but were added in the empirical formula to allow accurate determination of density and absorption coefficient. CCDC 1471203.

Total X-Ray Scattering PDF measurements.

Total scattering X-ray PDF experiments were performed at the National Synchrotron Light Source II (NSLS-II) on beamline 28-ID at Brookhaven

National Laboratory. The miniaturized sample (shown) was measured using the rapid acquisition pair distribution function (RaPDF) technique[56] with an X-ray energy of 65.7107 keV (=0.188682 Å). A Perkin Elmer 2D at panel detector (2048 × 2048 pixels and 200 × 200 μm pixel size) was mounted orthogonal to the beam path with a sample-to-detector distances of 300.785 mm. The raw 2D data were azimuthally integrated and converted to 1D intensity versus the magnitude of the scattering vector Q, ($Q = 2\pi\sin(\theta)/\lambda$=) using xPDFsuite[57] then corrected, normalized and Fourier transformed to obtain the PDF, G(r), using PDFgetX3.[58] A Ni standard was measured to calibrate the experimental setup with xPDF suite and fit with an FCC Ni model in PDFgui[43] to determine the instrumental resolution effects on the PDF, Q_{damp}=0.033039 $Å^{-1}$ and Q_{broad}=0.013760 $Å^{-1}$. Both miniaturized and crystalline (shown) samples were measured on a subsequent date with an X-ray energy of 67.3910 keV (= 0.183977 Å) and a detector distance of 207.6170 mm, giving instrumental resolution effects Q_{damp}=0.043902 $Å^{-1}$ and Q_{broad}=0.017594 $Å^{-1}$. The separate measurements of the miniaturized samples were consistent, but with better statistics collected on the former.

Cytotoxicity assays.

Human breast-cancer cells (MCF-7) and Human hepatocellular carcinoma cells (HepG2) were obtained from American Type Culture Collection (ATCC, Manassas, VA, USA). The cells were routinely cultured with DMEM F12 or DMEM (Invitrogen) containing 10% (v/v) heat-inactivated fetal bovine serum (FBS), at 37 ºC in a humidified (5%) CO_2 atmosphere. Growth inhibitory effects on cell lines were measured by the XTT (sodium 2,3,-bis(2-methoxy-4-nitro-5-sulfophenyl)-5-[(phenylamino)-carbonyl]-2H-tetrazolium inner salt) assay. Cells were plated at a density of 4 x 103 cells/well in 100 μL of culture medium in 96-well plates, and grown. After 24 hours incubation cells were treated with different concentrations of Gd-DOTA-4AmP and Zn-Gd-DOTA-4AmP nanoparticles during 24 hours and then, 20 μL of XTT was added. After 2 hours, the color formed was quantified with a spectrophotometric plate reader at 490 nm by a microplate reader (Victor3). The percentage of cell viability was calculated by dividing the average absorbance of the cells treated with the complex by that of the control. Each sample was tested in quadruplicate.

Relaxometry measurements.

Proton NMRD profiles were recorded on a Stelar SMARTracer Fast Field Cycling relaxometer (0.01-10 MHz) and a Bruker WP80 NMR electromagnet adapted to variable field measurements (20-80 MHz) and controlled by a SMARTracer PC-NMR console. The temperature was monitored by a VTC91 temperature control unit and maintained by a gas flow. The temperature was determined by previous calibration with a Pt resistance temperature probe. The longitudinal relaxation rates ($1/T_1$) were determined in physiological saline solution (NaCl, 0.9%) for colloidal suspensions of Zn-Gd-DOTA-4AmP nanoparticles ([Gd]=5.0 – 5.4 mM).

Acknowledgements

This work was supported by the MINECO-Spain through projects PN MAT2012-30994. I.I. and J.A.S. thank the MINECO for a RyC contract and a predoctoral FPU grant, respectively. J.A. is grateful to the Generalitat de Catalunya for a predoctoral FI grant. ICN2 acknowledges the support of the Spanish MINECO through the Severo Ochoa Centers of Excellence Program, under Grant SEV-2013-0295. M.T. acknowledges support from the U.S. Department of Energy NEUP #DE-NE 0000746 and S.J.L. Billinge for helpful discussion. Use of the National Synchrotron Light Source II, Brookhaven National Laboratory, was supported by the U.S. Department of Energy, Office of Science, Office of Basic Energy Sciences, under Contract No. DE-SC0012704. E. T. and C. S. Bonnet acknowledge financial support of the Ligue contre le Cancer (France).

Keywords: contrast agent • Gd(III) • chelates • coordination polymer • relaxometry

[1] A. S. Merbach, L. Helm, É. Tóth, *The Chemistry of Contrast Agents in Medical Magnetic Resonance Imaging*, John Wiley & Sons, **2013**.
[2] P. Caravan, J. J. Ellison, T. J. McMurry, R. B. Lauffer, *Chem. Rev.* **1999**, *99*, 2293–2352.
[3] S. Aime, M. Botta, E. Terreno, *Adv. Inorg. Chem.* **2005**, *57*, 173–237.
[4] E. Terreno, D. D. Castelli, A. Viale, S. Aime, *Chem. Rev.* **2010**, *110*, 3019–3042.
[5] M. Botta, L. Tei, *Eur. J. Inorg. Chem.* **2012**, *2012*, 1945–1960.
[6] J. Zhu, Z. Xiong, M. Shen, X. Shi, *RSC Adv.* **2015**, *5*, 30286–30296.
[7] J. Min, H. Jung, H.-H. Shin, G. Cho, H. Cho, S. Kang, *Biomacromolecules* **2013**, *14*, 2332–2339.
[8] M. B. Winter, P. J. Klemm, C. M. Phillips-Piro, K. N. Raymond, M. A. Marletta, *Inorg. Chem.* **2013**, *52*, 2277–2279.
[9] G. Zhang, J. Gao, J. Qian, L. Zhang, K. Zheng, K. Zhong, D. Cai, X. Zhang, Z. Wu, *ACS Appl. Mater. Interfaces* **2015**, *7*, 14192–14200.
[10] C. Diaferia, E. Gianolio, P. Palladino, F. Arena, C. Boffa, G. Morelli, A. Accardo, *Adv. Funct. Mater.* **2015**, *25*, 7003–7016.
[11] L. M. Randolph, C. L. M. LeGuyader, M. E. Hahn, C. M. Andolina, J. P. Patterson, R. F. Mattrey, J. E. Millstone, M. Botta, M. Scadeng, N. C. Gianneschi, *Chem. Sci.* **2016**, DOI: 10.1039/C6SC00342G.
[12] K. Zhang, M. Liu, X. Tong, N. Sun, L. Zhou, Y. Cao, J. Wang, H. Zhang, R. Pei, *Biomacromolecules* **2015**, *16*, 2618–2623.
[13] J. Della Rocca, W. Lin, *Eur. J. Inorg. Chem.* **2010**, *2010*, 3725–3734.
[14] J. Della Rocca, D. Liu, W. Lin, *Acc. Chem. Res.* **2011**, *44*, 957–968.
[15] P. Horcajada, T. Chalati, C. Serre, B. Gillet, C. Sebrie, T. Baati, J. F. Eubank, D. Heurtaux, P. Clayette, C. Kreuz, et al., *Nat. Mater.* **2010**, *9*, 172–178.
[16] W. J. Rieter, K. M. L. Taylor, H. An, W. Lin, W. Lin, *J. Am. Chem. Soc.* **2006**, *128*, 9024–9025.
[17] K. M. L. Taylor, A. Jin, W. Lin, *Angew. Chem. Int. Ed.* **2008**, *47*, 7722–7725.
[18] A. Carné-Sánchez, C. S. Bonnet, I. Imaz, J. Lorenzo, E. Tóth, D. Maspoch, *J. Am. Chem. Soc.* **2013**, *135*, 17711–17714.
[19] F. Avecilla, J. A. Peters, C. F. G. C. Geraldes, *Eur. J. Inorg. Chem.* **2003**, *2003*, 4179–4186.
[20] C. F. G. C. Geraldes, M. P. M. Marques, B. de Castro, E. Pereira, *Eur. J. Inorg. Chem.* **2000**, *2000*, 559–565.
[21] F. K. Kalman, M. Woods, P. Caravan, P. Jurek, M. Spiller, G. Tircsó, R. Kiraly, E. Brücher, A. D. Sherry, *Inorg. Chem.* **2007**, *46*, 5260–5270.
[22] K. J. Gagnon, H. P. Perry, A. Clearfield, *Chem. Rev.* **2012**, *112*, 1034–1054.
[23] G. V Martinez, X. Zhang, M. L. García-Martín, D. L. Morse, M. Woods, A. D. Sherry, R. J. Gillies, *NMR Biomed.* **2011**, *24*, 1380–1391.
[24] E. T. Clarke, A. E. Martell, *Inorganica Chim. Acta* **1991**, *190*, 27–36.
[25] S. Chaves, R. Delgado, J. J. R. F. Da Silva, *Talanta* **1992**, *39*, 249–254.
[26] X. Wang, T. Jin, V. Comblin, A. Lopez-Mut, E. Merciny, J. F. Desreux, *Inorg. Chem.* **1992**, *31*, 1095–1099.
[27] K. Kumar, C. A. Chang, L. C. Francesconi, D. D. Dischino, M. F. Malley, J. Z. Gougoutas, M. F. Tweedle, *Inorg. Chem.* **1994**, *33*, 3567–3575.
[28] E. T. Clarke, A. E. Martell, *Inorg. Chim. Acta* **1991**, *190*, 37–46.
[29] G. J. Fosmire, *Am. J. Clin. Nutr.* **1990**, *51*, 225–227.
[30] J. R. Curtis, G. C. Goode, J. Herrington, L. E. Urdaneta, *Clin. Nephrol.* **1976**, *5*, 61–65.

[31] C. L. Evans, *Br. J. Pharmacol. Chemother.* **1964**, *23*, 455–475.
[32] R. P. Singh, S. Kumar, R. Nada, R. Prasad, *Mol. Cell. Biochem.* **2006**, *282*, 13–21.
[33] L. Gaetke, *Toxicology* **2003**, *189*, 147–163.
[34] J. Aríñez-Soriano, J. Albalad, J. Pérez-Carvajal, I. Imaz, F. Busqué, J. Juanhuix, D. Maspoch, *CrystEngComm* **2016**, DOI: 10.1039/C5CE02520F.
[35] R. A. Coxall, S. G. Harris, D. K. Henderson, S. Parsons, P. A. Tasker, R. E. P. Winpenny, *J. Chem. Soc. Dalt. Trans.* **2000**, 2349–2356.
[36] R. Fu, X. Huang, S. Hu, S. Xiang, X. Wu, *Inorg. Chem.* **2006**, *45*, 5254–5256.
[37] S. Drumel, P. Janvier, P. Barboux, M. Bujoli-Doeuff, B. Bujoli, *Inorg. Chem.* **1995**, *34*, 148–156.
[38] L. Di Bari, G. Pescitelli, A. D. Sherry, M. Woods, *Inorg. Chem.* **2005**, *44*, 8391–8398.
[39] R. S. Dickins, D. Parker, J. I. Bruce, D. J. Tozer, *Dalt. Trans.* **2003**, 1264–1271.
[40] S. J. L. Billinge, T. Egami, *Underneath the Bragg Peaks, 2nd Edition*, Pergamon, **2012**.
[41] P. K. Allan, K. W. Chapman, P. J. Chupas, J. A. Hriljac, C. L. Renouf, T. C. A. Lucas, R. E. Morris, *Chem. Sci.* **2012**, *3*, 2559–2564.
[42] M. I. Mohideen, P. K. Allan, K. W. Chapman, J. A. Hriljac, R. E. Morris, *Dalton Trans.* **2014**, *43*, 10438–10442.
[43] C. L. Farrow, P. Juhas, J. W. Liu, D. Bryndin, E. S. Božin, J. Bloch, T. Proffen, S. J. L. Billinge, *J. Phys. Condens. Matter* **2007**, *19*, 335219.
[44] T. Vitha, V. Kubícek, P. Hermann, L. Vander Elst, R. N. Muller, Z. I. Kolar, H. T. Wolterbeek, W. A. P. Breeman, I. Lukes, J. A. Peters, *J. Med. Chem.* **2008**, *51*, 677–683.
[45] N. Raghunand, C. Howison, A. D. Sherry, S. Zhang, R. J. Gillies, *Magn. Reson. Med.* **2003**, *49*, 249–257.
[46] M. L. Garcia-Martin, G. V Martinez, N. Raghunand, A. D. Sherry, S. Zhang, R. J. Gillies, *Magn. Reson. Med.* **2006**, *55*, 309–315.
[47] M. M. Ali, M. Woods, P. Caravan, A. C. L. Opina, M. Spiller, J. C. Fettinger, A. D. Sherry, *Chem. Eur. J.* **2008**, *14*, 7250–7258.
[48] Z. Shanrong, W. Kuangcong, D. Sherry, *Invest. Radiol.* **2001**, *36*, 82–86.
[49] G. Guerrero, J. G. Alauzun, M. Granier, D. Laurencin, P. H. Mutin, *Dalton Trans.* **2013**, *42*, 12569–12585.
[50] G. J. M. Koper, M. Borkovec, *Polymer (Guildf).* **2010**, *51*, 5649–5662.
[51] A. Barge, G. Cravotto, E. Gianolio, F. Fedeli, *Contrast Media Mol. Imaging 1*, 184–188.
[52] J. Juanhuix, F. Gil-Ortiz, G. Cuní, C. Colldelram, J. Nicolás, J. Lidón, E. Boter, C. Ruget, S. Ferrer, J. Benach, *J. Synchrotron Radiat.* **2014**, *21*, 679–689.
[53] W. Kabsch, *J. Appl. Crystallogr.* **1993**, *26*, 795–800.
[54] L. Palatinus, G. Chapuis, *J. Appl. Crystallogr.* **2007**, *40*, 786–790.
[55] G. M. Sheldrick, *Acta Crystallogr. A.* **2008**, *64*, 112–122.
[56] P. J. Chupas, X. Qiu, J. C. Hanson, P. L. Lee, C. P. Grey, S. J. L. Billinge, *J. Appl. Crystallogr.* **2003**, *36*, 1342–1347.
[57] X. Yang, P. Juhas, C. L. Farrow, S. J. L. Billinge, *arXiv* **2015**, 1402.3163v3.
[58] P. Juhás, T. Davis, C. L. Farrow, S. J. L. Billinge, *J. Appl. Crystallogr.* **2013**, *46*, 560–566.

Entry for the Table of Contents

Layout 1:LL PAPER

A coordination polymer has been synthesized by using a stable Gd(III) chelate in order to prevent any fortuitous release of free lanthanide ion. The use of this chelate as a linker in the coordination polymer allows enhancing the relaxometric properties (maximum r_1=16.4 $mM^{-1}s^{-1}$ at 10 MHz) and the pH responsiveness (Δr_1 = 108% between pH 4 and 6.5), beyond the values obtained for the Gd(III) chelate itself.

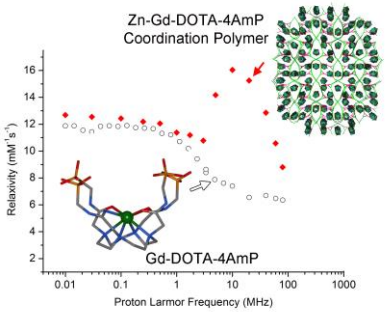

Javier Aríñez-Soriano, Jorge Albalad, Arnau Carné-Sánchez, Célia S. Bonnet, Félix Busqué, Julia Lorenzo, Jordi Juanhuix, Maxwell W. Terban, Inhar Imaz, Éva Tóth, Daniel Maspoch**

Page No. – Page No.

pH-responsive relaxometric behaviour of coordination polymer nanoparticles made of a stable macrocyclic gadolinium chelate